Full-field deformation characteristics of anisotropic marble under compression revealed by 3D digital image correlation

Y. Wang[1*], Z. Y. Song[1], Z. Q. Hou[1], C. Zhu[2]

1.Beijing Key Laboratory of Urban Underground Space Engineering, Department of Civil Engineering, School of Civil & Resource Engineering, University of Science & Technology Beijing, Beijing 100083, China.
2. School of Earth Sciences and Engineering, Hohai University, Nanjing, 210098, China

Abstract: This work aims to reveal the anisotropic full-field displacemnet and the progressive failure behaviors of interbedded marble under uniaxial compression using three dimensional digital image correlation (3D DIC) technique. The effects of the interbed orientation on the field displacement and strain pattern and the crack evolution were analyzed qualitatively and quantitatively. Testing results show that different stress strain responses can be generated depending on the interbed orientation, and the interbeds influence the localized deformation and high strain concentration pattern. The field displacement evolution curves present different pattern and are impacted by the localized deformation. In addition, the strain localization takes places progressively and develops at a lower rate for rock with 0° and 90° interbed than those of 30° and 60° interbed rock. The quick shear-sliding along the interbed leads to the minimum strength of rock having 30° interbed orientation. It is suggested that rock anisotropic field deformation is structure depended.

Keywords: 3D DIC; Full-field deformation; Interbeds; Strain localization

Corresponding author:

Y. Wang, Associate professor

Address: 30 Xueyuan Road, Haidian District, Beijing 100083 P. R. China

Tel: +86 18046522933

Email:good541571889@126.com; wyzhou@ustb.edu.cn

1. Introduction

Rock contains various discontinuities, e.g., layers, joints, faults, foliations and cleavages, etc., which predominantly impact its deformation and failure mode [1-3]. The interbed structure as a typical discontinuity unit is commonly encountered in nature for many kinds of rock, e.g., shale, mudstone, marble, carbonate, anhydrite, or slate, etc. Geometrical characteristics of interbeds including thickness, inclination angle and spacing determine the initiation and propagation of new cracks in rocks, which in turn leads to the non-linear deterioration of rock structure and eventually structural failure. In addition, different patterns of interbeds in terms of orientation and ligament angle can result in different failure mode (tension or shear) and influence the whole fracture evolution. As a result, it is of great importance to investigate the anisotropic fracturing behavior of interbedded rocks.

Many studies have been performed to reveal the anisotropic geomechanical behaviors of interbedd rock with respect to deformation, strength, elastic modulus, velocities, failure mode, etc. Liu et al. [4] simulated a clayed interbed by a Cam clay model to study the fluid injection responses and the final surface deformation pattern depends on interbed swelling potential. Cata et al. [5] reveals the influence of anhydrite interbed on the stability of a storage carven in Mechelinki salt deposit (Northern Poland). Ozturk and Altinpinar [6] carried out point load test to determine the strength and interbedded rock and found that rock strength shows obvious anisotropy. Wang et al. [7] reveals the deformation characteristics of rock salt with mudstone interbeds surrounding gas and oil storage cavern, they pointed that the extension of plastic and dilatancy zones in rock salt was impacted by the interbed structure. Tommasi et al. [8] employed distinct element modelling to investigated the influence of clayed interbeds in limestone formation on rock avalanches produced by planar rockslides, the instability process was detailed studied. Zhao et al. [9] performed hydraulic fracturing tests on continental shale with interbeds, the influences of the interbed geometrical parameters on fracture network propagation were revealed. Wang et at. [10] performed numerical studies for interbedded shale to exam the interbed configuration on rock fracturing subjected to hydraulic fracturing. Wang et al. [11] conducted uniaxial compressive test combined with real-time acoustic emission (AE) monitoring to reveal the anisotropic fracture and energy evolution during rock failure. They found that the AE patterns are strongly impacted by interbed structure. Meanwhile, Wang et al. [12-13] conducted cyclic or fatigue loading test on interbedded marble, the experimental results shows that the fatigue lifetime of rock also depends on interbed orientation. They found that the damage evolution and irreversible deformation during cyclic loads determine the final failure mode. The above investigations reveal that the interbed structure alters the crack propagation pattern and the associated rock instability mode. To quantitatively study the influence of interbed on rock fracturing, non-destructive approaches, such as ultrasonic pulse velocity measurement [14], AE monitoring [15-16] and X-ray computed tomography [17-19] have been employed to capture the fracturing process.

However, those methods employed to monitor rock failure is hard to detect the deformation and strain development, and the proper measurement of deformation and strain evolution in interbedded rock are crucial to understanding the stress strain feature and the early identification of structural deterioration.

The strain localization and evolution, and onset of fracture were crucial to the rock mass stability prediction. Recently 3D digital image correlation (DIC) technique was introduced in the rock mechanics field, and 3D DIC has been successfully applied to investigate the deformation behaviors of rocks. Tang et al. [20] developed a measuring method using 3D DIC for rock under triaxial compression, and the progressive failure behaviors and crack evolution were analyzed. Munoz et al. [21] reveals the pre-peak and post-peak strain responses of rock during uniaxial compression using 3D DIC, the field of strains and eventual strain localization in the rock surface were analyzed. Sharafisafa et al. [22] performed 3D DIC measurement for pre-flawed rock-like material during rock deformation, the influence of flaw configuration on crack evolution was investigated. Xing et al. [23] employed high-speed 3D DIC for rock subjected to dynamic loads, the initiation of crack from strain localization and the failure mode were revealed in detail. Munoz and Taheri [24] carried out 3D DIC measurement to investigate the sample aspect ratio and field strain development of sandstone under uniaxial compression, the development rate of localized band pre- and post-peak failure were studied. All these attempts on DIC fracture studies demonstrated the robustness and usefulness of this method in characterizing and detecting different types of cracks and failures in rock. However, the use of 3D DIC in rock fracture analysis was mainly limited to intact rock, pre-flawed rock, or rock-like material. There are few investigations on the field strain development and fracture evolution for interbedded rocks under compression using 3D DIC technique.

To fill this gap, a series of uniaxial compressive tests were performed on interbedded marble samples obtained from an open pit slope to explore the influence of interbed structure on the progressive failure behaviors of rocks. The anisotropic displacement and strain evolution were presented and discussed. Furthermore, the displacement or strain responses inside or outside the localized zone were analyzed qualitatively and quantitatively based on the measured results of 3D DIC technique.

2. Experimental study

2.1. Rock type and sample preparation

The tested rocks with interbeds were obtained from a North open pit mine slope at the Jiama mining, Tibet, Northwest of China, as shown in Fig.1. The rock shows strong nonhomogenity and heterogeneity, apart from the interbed structure, pyrite bands can also be observed from the outcrop. Relative fresh rock blocks were obtained from the blasting zone of the stepped slope. Apart from the macroscopic observation of the interbed structure in the rock mass outcrop, laboratory scanning electron microscope (SEM) testing also reveals the mesoscopic interlayers within the

tested marble, as shown in Fig.2. The BSE-SEM picture clearly shows the interbeded structure, owing to the differential composition of the rock matrix and interlayer, they displays different color in the SEM picture. In addition, plenty of white speckles were observed and they are the pyrite mineral distributed internal marble. The XRD analysis reveals the mineral composition, and its main mineral components include quartz, anorthite, biotite and a little amount of calcium manganese. In order to perform 3D DIC testing, all the tested rock samples were prepared as cylindrical shape with the diameter of 50 mm and height of 100 mm according to the recommended method by ISRM. The tested rock samples were polished to ensure that the parallelism and the non-uniformity error is less than 0.1mm and 0.05 mm, respectively.

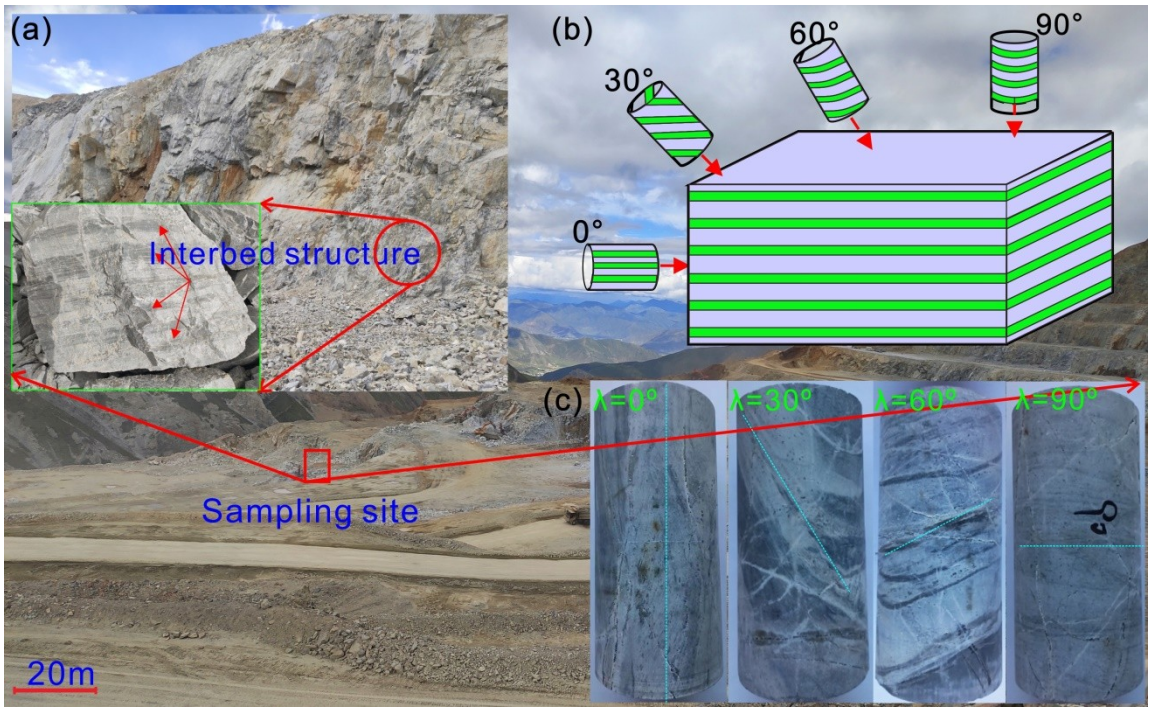

Fig.1 Rock sampling site from the North open pit slope in the Jiama copper polymetallic mine. (a. The open pit mine slope; b. Scheme of the preparation of rock samples with different orientations; c. Reprehensive rock samples used in this work)

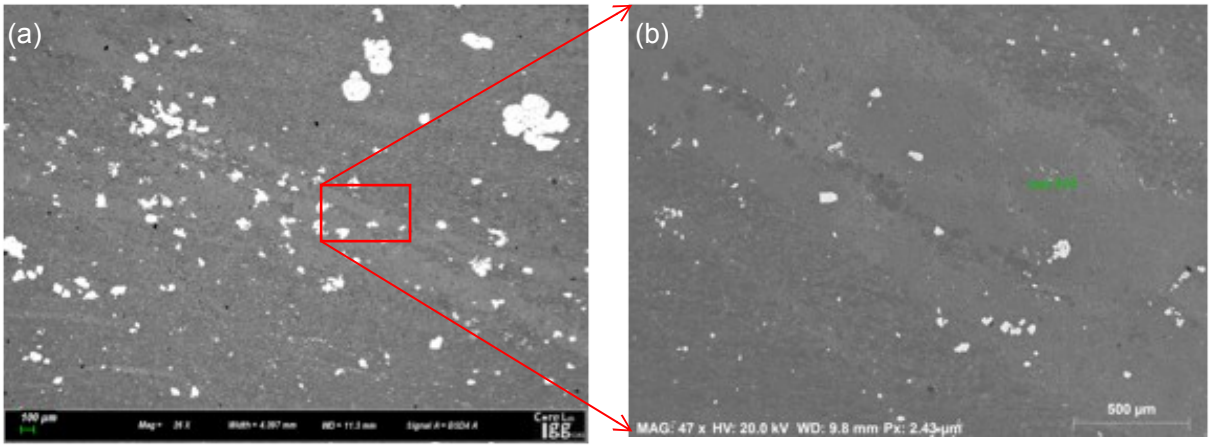

Fig.2 Description of the mesoscopic structure of interbed marble (a. Typical SEM picture to observe the non-homogenous structure; b. Magnification of the red box in Fig.2a)

2.2. Testing apparatus

The testing devices employed in this work include the mechanics testing system the 3D DIC system. As illustrated in Fig.3, the normal stress is applied by a SANS material testing machine with its maximum axial load of 1500 kN, the loading rate was set to be 0.06mm/min for rock exposed to static loading conditions. Meanwhile, the 3D DIC system was used to capture the fracturing process of rock in order to get the full-field displacement and strain evolution. The DIC system is mainly composed to two high speed camera characterized with a charge-coupled device (CCD), two light sources, a set of camera tripod and imaging acquisition computer. The light source was installed in front of the tested marble samples to improve the image acquisition quality.

A FLIR black & white CCD camera with a resolution of 2100 ×2100 pixels is employed to capture images. Before the tests, the speckle pattern on the marble samples was created by first spraying ordinary white paint and then by tarnishing black paint on rock surface. A self-developed image processing system of RFAC-DIC3D is used to analyze the captured images. Based on the previous used estimation method [25, 26], the camera covers a range of 50 mm ×100 mm through the viewing window, which can be converted into 50/2100=0.023 mm/pixel×0.023 mm/pixel.

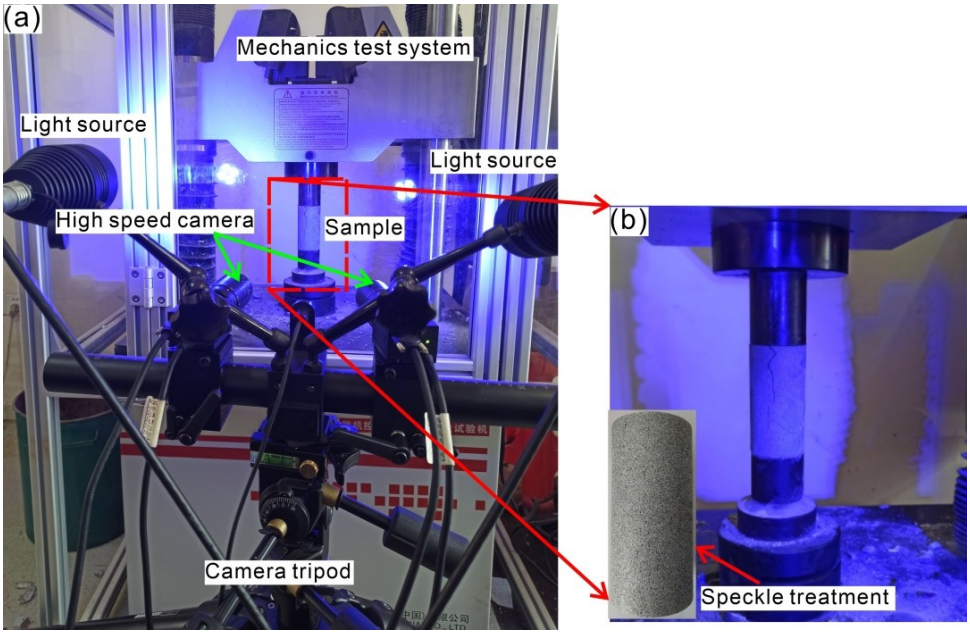

Fig.3 The experimental apparatus in this work. (a. The testing system mainly composed of the material rock mechanics machine, high speed camera, light source, camera tripod ; b. Preparation of speckle on the marble samples)

2.3. 3D DIC method

The 2D DIC measures the in-plane strain and displacement, assuring that the tested rock sample is planar and its deformation is within the object plane (i.e., facing to the high speed camera). The 2D DIC results are impractical to be applied to cylindrical-shaped rock samples, as rock deformation occurs in three-dimensional space and not limited in-plane [24].

The 3D DIC technique uses two cameras (Camera 1 and Camera 2) to simultaneously record the image points from two different angles to recover the 3D position, allowing the omni-directional measurement of the 3D shape and displacement, as shown in Fig. 4. For example, there are two three-dimensional points (M and N) on the same projective ray and the same projective point (M) on the image plane 1.There's an infinite number of three dimensional points that correspond to the projective point M. If there are two projective points (m, m '), then the only point corresponds to m. Similarly, projective points (m, n') correspond to a unique point N. After taking a series of images of the surface pattern, the first image was regarded as the reference image (undeformed). The subsequent images were regarded as the deformed images. The three-dimensional positions of these points are confirmed, thus creating a three-dimensional measurement of the sample shape. The strain field of undeformed and deformed states was compared by using DIC software [26-27].

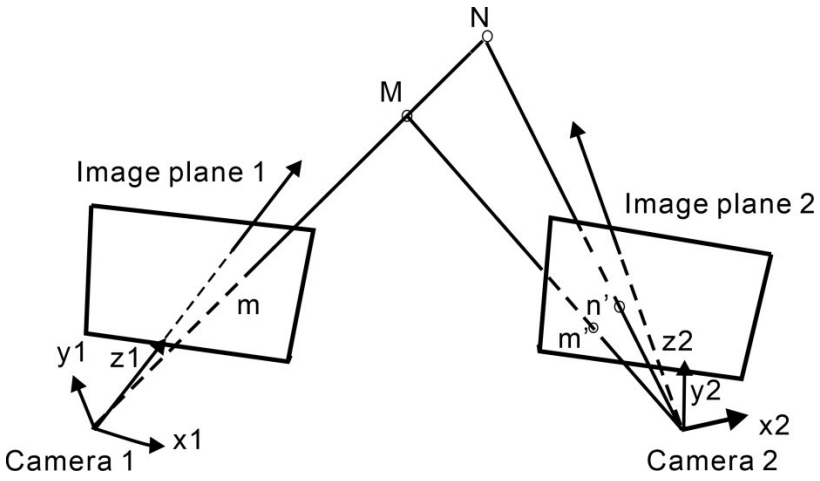

Fig.4 Scheme diagram of the third dimension imaging by two cameras

3. Results analysis

3.1. Representive stress strain curves

Typical stress strain curves for the interbedded marble are shown in Fig.5. As illustrated in Fig.5a, the peak strength and peak strain displays obvious anisotropy, and the stress is the maximum and minimum for a sample with 0° and 30° interbed orientation. All the rock samples present strong brittle failure and the peak strain is less than 1%. It is interesting that the growth of the axial stress strain curves does not show a monotonous pattern, a fluctuation phenomenon can be seen apart from the 30° orientation sample. The reason for the fluctuation is that the tested marble

contains natural fractures within them, the pre-existing natural fracture is the weakest parts and the stimulation of the natural fracture alters the stress distribution on rock samples. Fig.5b shows the anisotropic strength and strain for the tested samples, and a "V" change trend is found. Summarization of basic physical and mechanical parameters of all the tested samples is listed in Table 1.

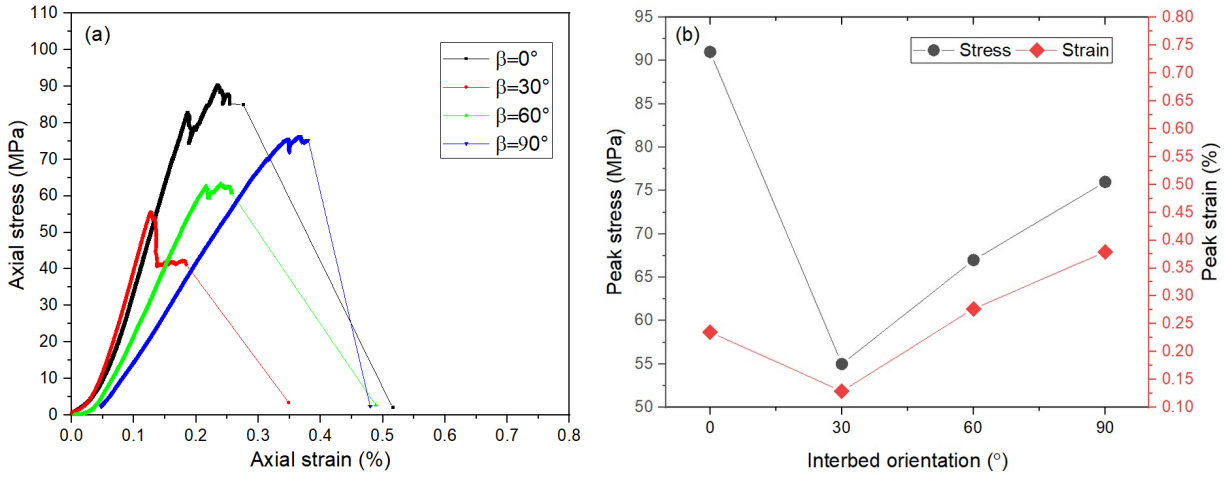

Fig.5 Typical stress strain responses for the marble samples (a. Stress strain curves for marble samples with different interbed orientation; b. Comparison of peak stress and strain for the the tested samples)

Table 1 Summarization of the physical and mechanical properties of the tested marble

Rock ID	L×d (mm×mm)	Density (g/cm^3)	UCS (MPa)	Peak strength, σ_c (MPa)	Peak strain, ε_c (%)	E_0 (GPa)	P-wave velocity (m/s)	S-wave velocity (m/s)
M0-1	99.75×49.59	2.784	91.65	95.04	0.236	34.45	5045	4065
M0-2	99.39×49.88	2.764	100.25	100.23	0.261	36.66	4966	3971
M30-1	99.95×49.32	2.810	55.25	74.56	0.281	31.05	4665	3756
M30-2	99.19×49.66	2.778	40.24	70.35	0.277	29.55	4408	3569
M60-1	100.01×50.02	2.749	67.41	59.23	0.370	25.32	4235	3402
M60-2	99.98×49.77	2.743	71.33	60.23	0.412	23.65	4287	3411
M90-1	99.66×49.85	2.716	76.89	45.85	0.437	20.45	3989	3187
M90-2	100.02×49.17	2.825	88.65	45.77	0.534	19.98	4005	3204

3.2. Descriptoin of field displacement evolution characteristics

As described in the testing method, a three-dimensional DIC analysis is used in this work, therefore, the spatial deformation of rock surface faced to the high speed camera can be obtained. Fig.6a shows the displacement of the tested marble in Z-

direction, i.e., the orientation vertical to the loading direction. A total of eight represented evolution stages are selected for each sample at different loading level. It can be seen that the evolution of Z-displacement shows obvious difference owing to the existing of interbeds and also the natural fracture. For rock sample with a 0° interbed orientation, the interlayer are parallel to the normal stress, the lateral spalling results in the volumetric expansion and the Z-displacement is relatively larger than other cases. Especially, the Z-displacement in the upper part is larger than the lower part, this result indicates that the tensile splitting is obvious for the upper part of rock. In addition, the Z-displacement value is opposite indicating that the volumetric expansion orientation at the upper and lower part of the sample is opposite, i.e., one part points to the camera and the other part deviate from the camera. Moreover, macroscopic spalling occurs at the left of the sample when axial stress reaches to the peak strength. As illustrated in Fig.6b, for a sample with 30° interbed orientation, the Z-displacement display a triangular concentration zone at the top left of rock sample, shown as dark blue color. At the left middle part of rock sample, a relatively large deformation zone can also be observed, marked with rectangular box. The differential displacement indicates the occurrence of larger sliding along the contact surface of interlayers. The sliding trend becomes more and more obvious until rock failure, and spalling of rock blocks indicates the coalescence of the sliding surface (Fig.6b-8). As illustrated in Fig.6c, the Z-displacement evolution process also clearly shows the rock expansion characteristics, and a concentration zone is observed (red color in Fig.6c-4,5,6,7,8). The large deformation at the lower right part indicates the formation of localized band. At rock failure stage, owing to the instability of the localized band 1, two other failure surfaces emerge. For the sample having an interbed orientation of 90°, it is hard to observe obvious Z-displacement and the rock is compacted during the whole loading process. This result indicates that the compaction deformation of rock with 90° interbed occupies a major percentage. In addition, The Z-displacement at lower part is larger than that of the top part, the differential deformation becomes stronger and stronger.

The total displacement evolution patterns that consider the three-dimensional deformation of marble are shown in Fig.7. The total displacement results demonstrate rock deformation at X,Y,Z directions. For rock with a 0° interbed orientation in Fig.7a, the total displacement of rock right side is larger than the left side owing to the spalling in the left top of rock. Large displacement zone is observed to be located at the natural fracture (i.e., pyrite band). In Fig.7b, the differential total displacement field is clear to display the localized deformation along a 30° orientation. The localized deformation becomes more and more obvious as loading increases. The right part of this sample resist axial loading. In Fig.7c for the sample having a 60° interbed orientation, localized deformation band inclines about 30° to the horizontal plane. The total displacement is relatively large above the localized band. At the final loading stage, another localized band parallel to loading direction is also observed. For the marble sample with a 90° interbed orientation, the densification effect plays a dominant role, and the displacement in the lower part is

larger than the upper part. For this sample with horizontal interbeds, the compaction vertical to the normal stress is stronger than the other samples.

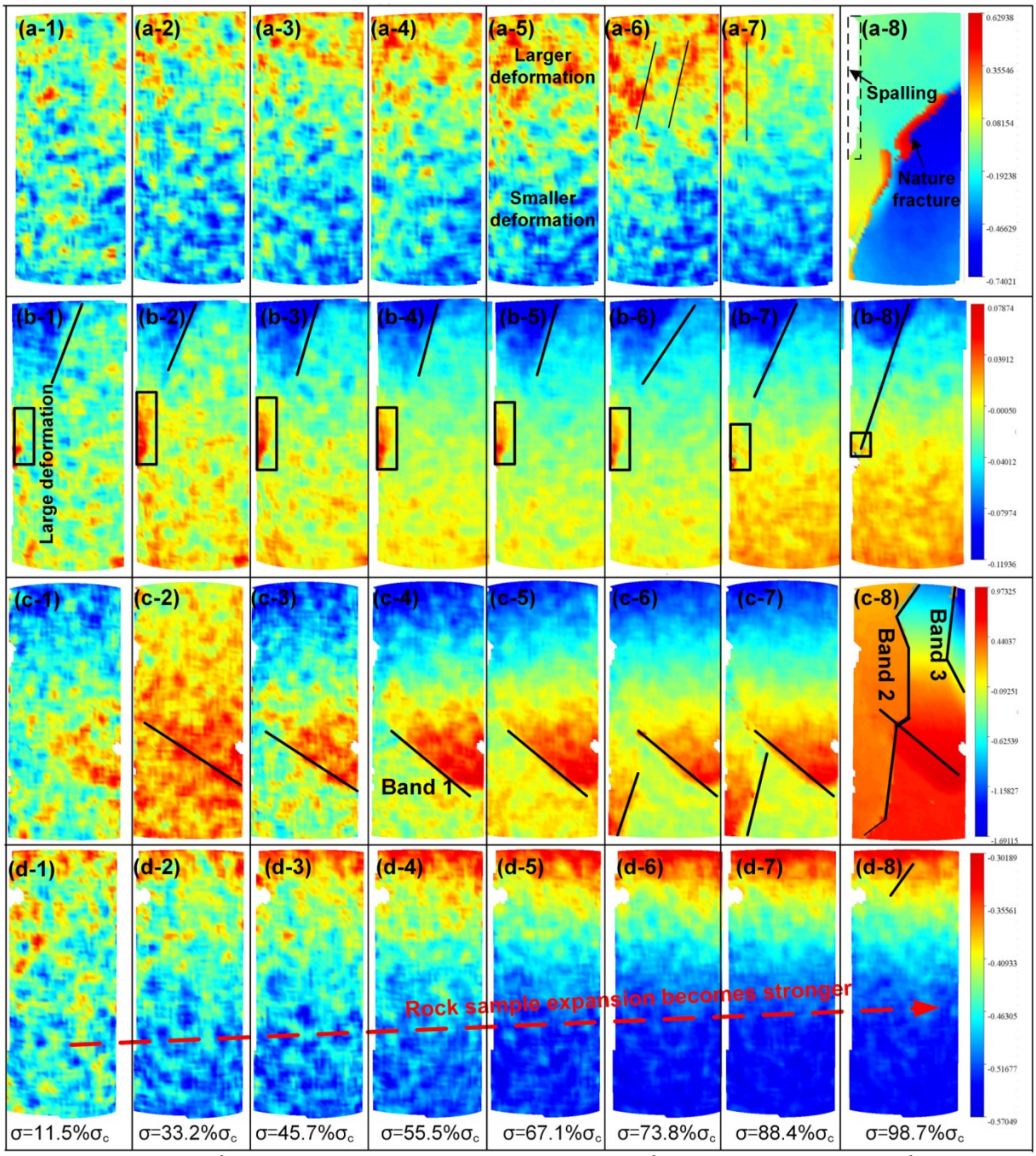

Fig.6 Evolution of the Z-direction displacement field for the marble samples with different interbed orientations, 8 loading stages are selected during the whole deformation process, labeled "1-8", the stress level is 0.115, 0.332, 0.457, 0.555, 0.671, 0.738, 0.884 and 0.987 times of the peak

stress. a-d: The interbed orientation is 0°, 30°, 60°, and 90°, respectively.)

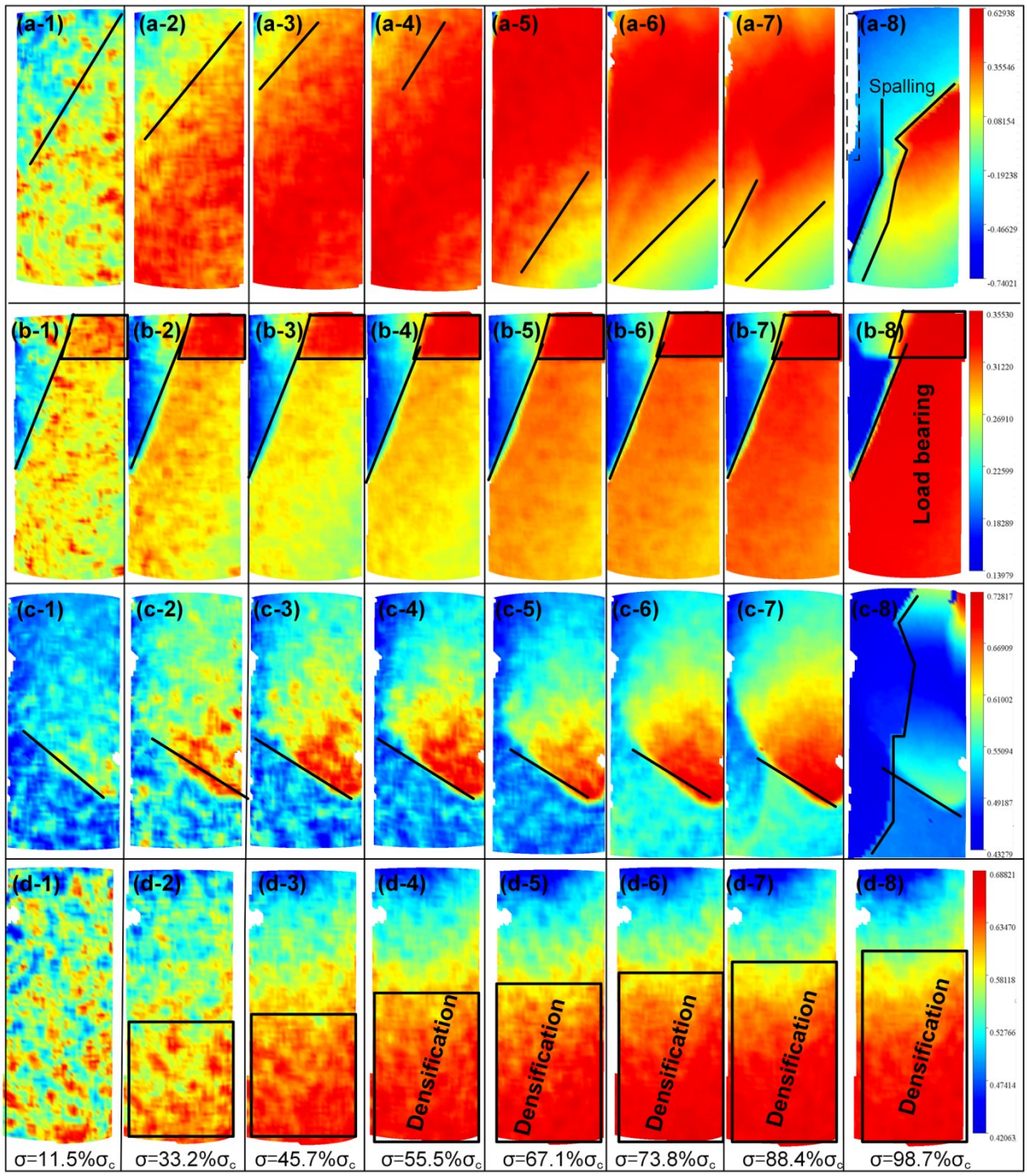

Fig.7 The field total displacement evolution for the marble sample with different interbed orientations, 8 loading stages are selected during the whole deformation process, labeled "1-8", the stress level is 0.115, 0.332, 0.457, 0.555, 0.671, 0.738, 0.884 and 0.987 times of the peak stress. (a-d: The interbed orientation is 0°, 30°, 60°, and 90°, respectively.)

3.3. Descriptoin of field strain evoltuion characteristics

As stated above, the pre-existing of the interbed structure has obvious impact on the displacement evolution. The strain in XY plane is plotted in Fig.8. For a sample

having an orientation of 0° in Fig.8a, at the initial loading stage, the strain concentration band is parallel to loading direction. Because of the weak strength of contact among the interlayers and also the natural fracture, rock shows splitting failure and the high strain bands along the natural fractures. For sample with a 30° interbed orientation in Fig.8b, an obvious strain concentration band forms that having a 30° inclination with respect to loading direction. For sample with a 60° interbed orientation in Fig.8c, at the loading stages of 1 to 6, only one strain localized band is observed; however, strain band branches at the 7^{th} loading stage. Apart from the shear strain band, a tensile strain band forms for this sample. Fig.8d plots the XY-strain evolution for sample having a 60° interbed orientation, it shows that multiple strain bands parallels to each other and a tensile band forms at rock failure stage. The result in Fig.8d implies that the stiffness difference between the rock matrix and interlayers leads to the concentration of strain bands.

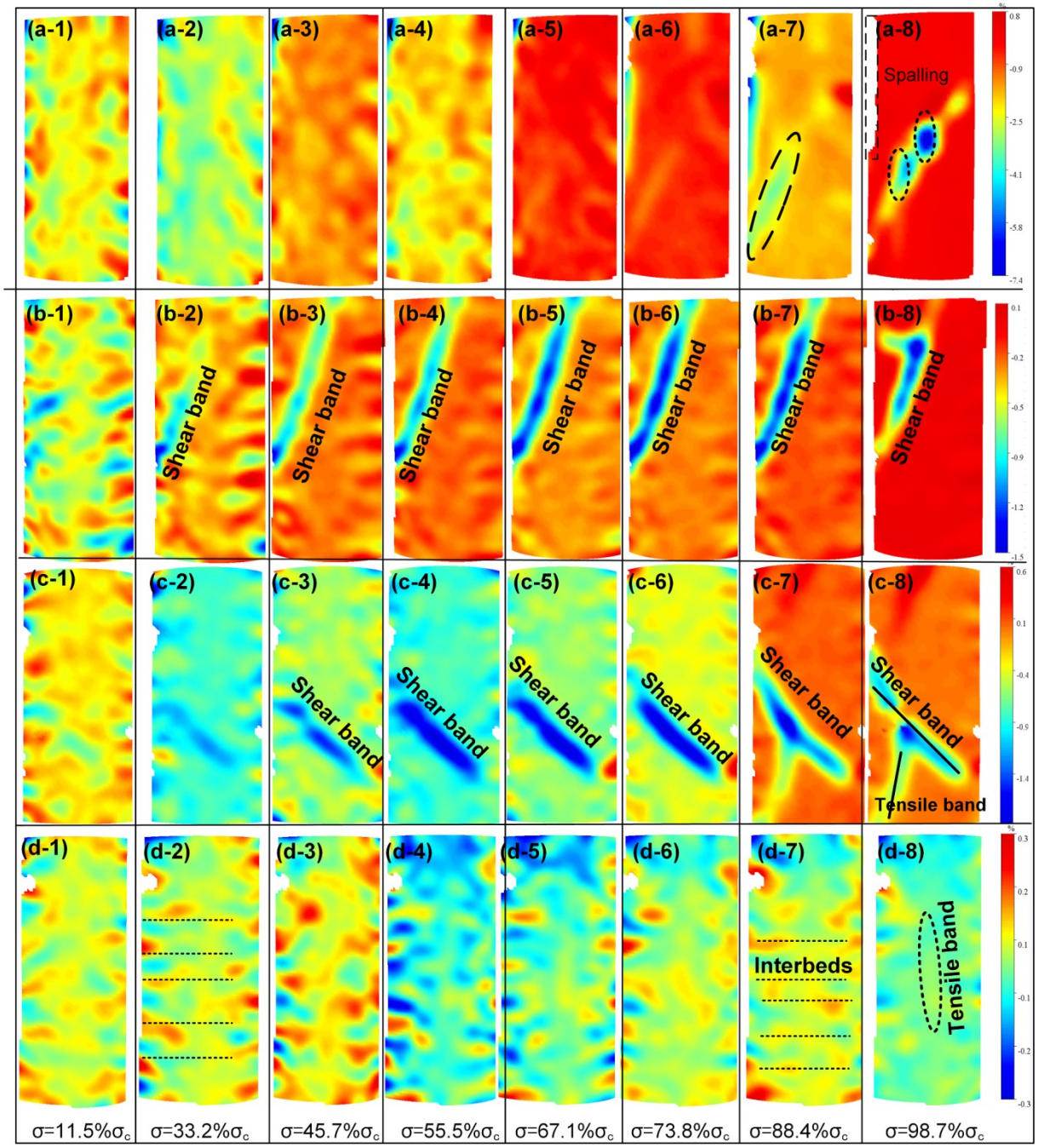

Fig.8 Evolution of the principal strain in XY plane for the marble sample with different interbed orientations, 8 loading stages are selected during the whole deformation process, labeled "1-8" , the stress level is 0.115, 0.332, 0.457, 0.555, 0.671, 0.738, 0.884 and 0.987 times of the peak stress. The interbed orientation is 0°, 30°, 60°, and 90°, respectively)

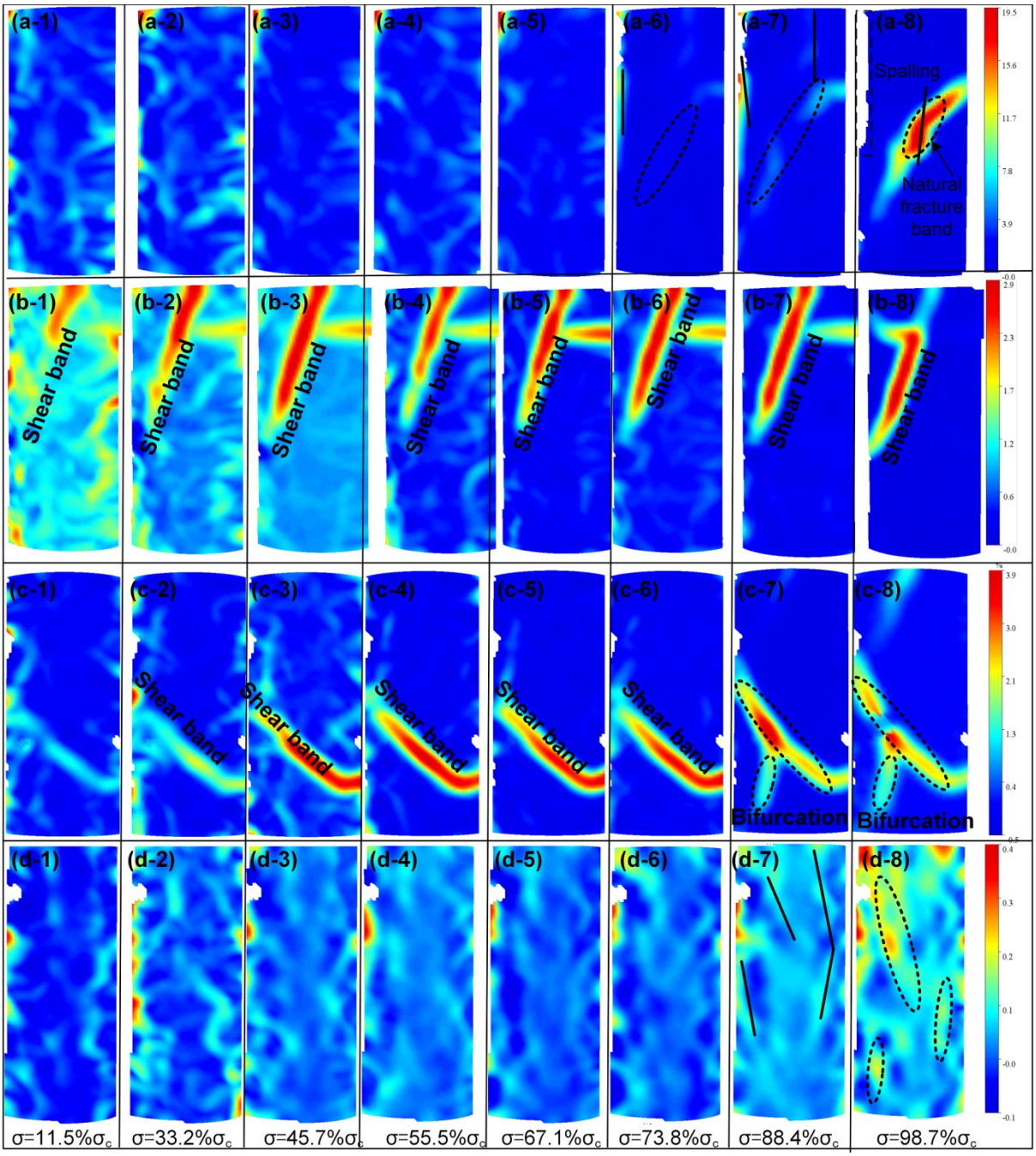

Fig.9 Evolution of the principal strain for the marble sample with different interbed orientations, 8 loading stages are selected during the whole deformation process, labeled "1-8", the stress level is 0.115, 0.332, 0.457, 0.555, 0.671, 0.738, 0.884 and 0.987 times of the peak stress. (a-d: The interbed orientation is 0°, 30°, 60°, and 90°, respectively)

The evolution of principal strain is also plotted in Fig.9. The maximum strain band shows obvious difference for rock samples having different structure, i.e., the interbed orientation impacts the stress distribution and pattern of high strain band. The failure for rock with 0° interbed orientation is tension mode but impacted by the pre-exisitng natural fracture. A mixed of tension-splitting and shear failure occurs for rock sample with a 60° and 90° interbed orientation. Shear failure dominates the

whole failure process for rock having 30° interbed orientation. For rock with 60° interbed orientation, strain band bifurcation phenomenon is found at the 7th loading stage. High strain concentration band parallel to loading direction is observed for rock with 90°interbed orientation, indicating the tension failure for this sample. In addition, the evolution pattern of the localized band indicates that the developing rate of strain localized band is quicker for rock having an interbed orientation of 30° and 60° than the other cases.

3.4. Monitoration of field displacemnt evoluiton

In order to well reveal the anisotropic strain evolution characteristics, the evolution of displacement field at key points and typical sections are analyzed. Reprehensive monitoring pints and lines are marked in the displacement contour in Fig.10. Fig.10 plots the relationship between the Z-displacement, total displacement and section length. Although the three monitoring lines (Line 0,1,2) are set at the same height of rock sample, the change of the Z-displacement and total displacement is different. In Fig.10a, impacted by the pre-existing natural fracture, displacement skips along the section. The growth of the total displacement shows a first steady, and then a quick increase and then a steady pattern. The sudden increase of displacement is attributed to the natural fracture. The displacement at the middle part (line 0) is relatively large compared to the other two monitoring lines. The Z-displacement curve skips strongly for Line 0 and Line 1, indicating the formation of large deformation zone. As illustrated in Fig.10b for rock sample having an 0° interbed orientation, it is obvious that two types of distinct change trend is observed. At the sliding zone that is covered with blue color, its displacement is larger than the red zone. This result indicates that failure of this sample is only the shear sliding along the interbed, one main failure surface is for this sample. As illustrated in Fig.10c for rock sample having an 60° interbed orientation, the fluctuation of displacement curves is severe than other cases, displacement presents a sudden skips at the concentration band. The Z-displacement and total displacement becomes large after crossing the displacement concentration band. As shown in Fig.10d, as the monitoring line is parallel to the interbed orientation, the Z-displacement and total displacement curve both grow steady. The results of the displacement evolution in Fig.10 further confirm the influence of interbeds on rock deformation.

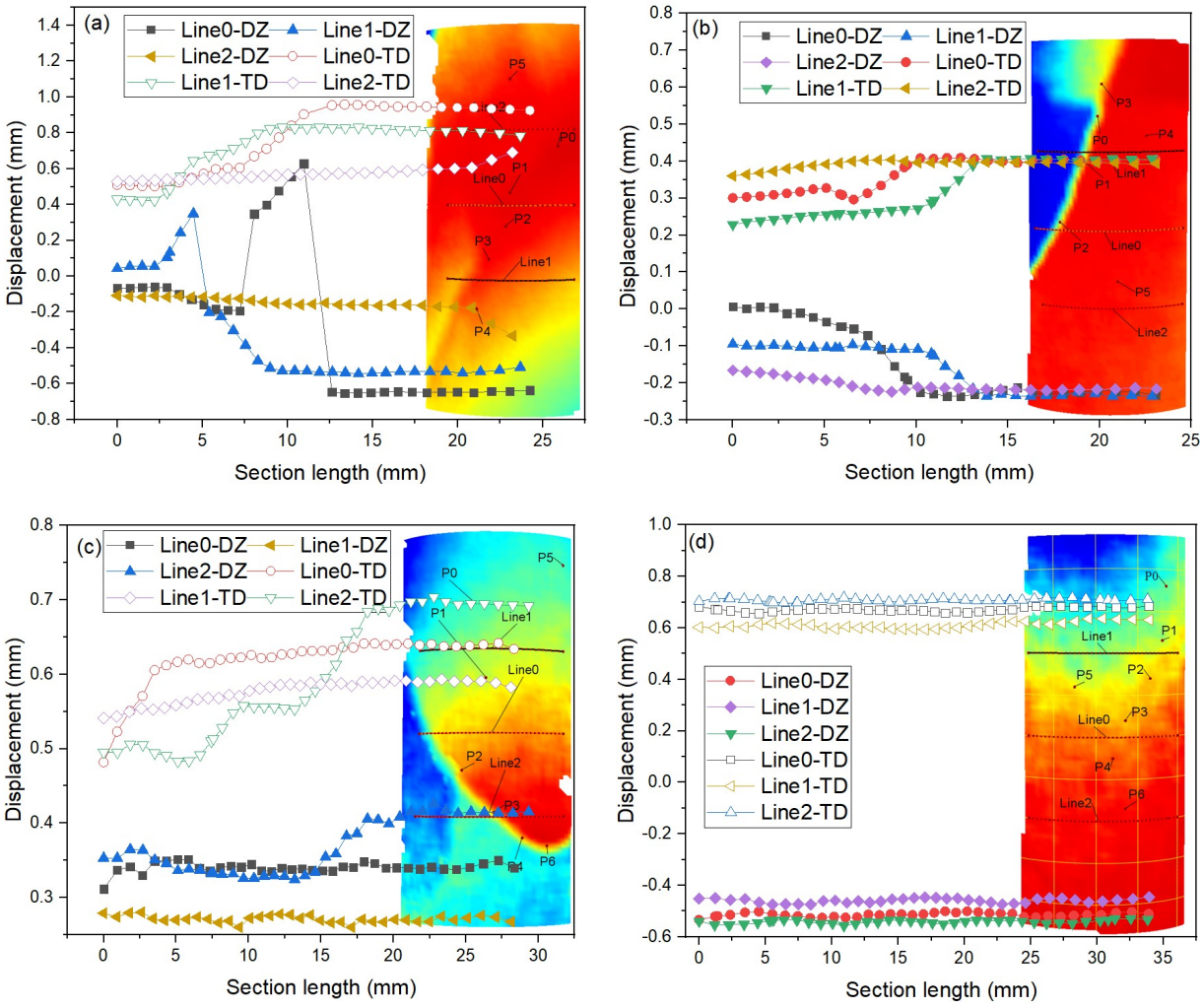

Fig.10 Field displacement evolution during rock deformation for the monitoring lines (Line1, 2, 3). (a-d: Marble with interbed orientation of 0°, 30°, 60°, and 90°, respectively)

Several key points along the displacement concentration band and at the top or low part of rock sample were chosen to reveal the evolution process, as shown in Fig.11. For the points in the concentration band, i.e, point 1, 3, 5 for 0° interbed orientation, point 0, 1, 3 for 0° interbed orientation, point 2,3,4,6 for 0° interbed orientation, and point 2, 3, 4 for for 90° interbed orientation, the displacement curves present different evolution trend. The enlarged figures can well demonstrate the change of the displacement in the region of interest. The change of displacement in the monitoring point is influenced by the interbed structure, and the value of the points at the concentration band is larger than other points. It is interesting to observe that the Z-displacement and the total displacement for the sample with 30° interbed orientation is larger than other samples, indicating that this sample is easy to failure and exhibiting low strength. The shear sliding along the interbed results in the instability of this sample.

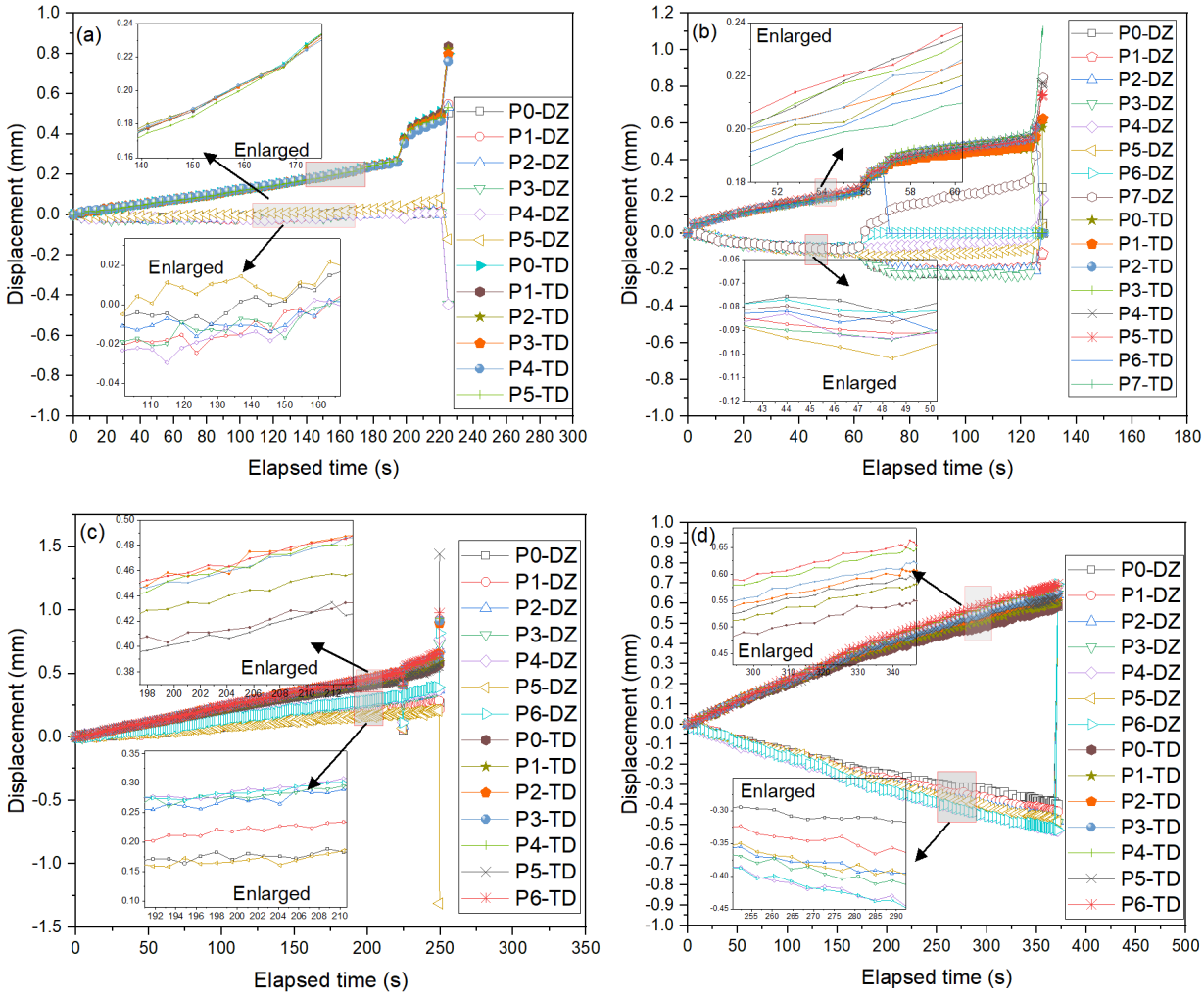

Fig.11 Field displacement evolution for the key monitoring points. (a-d: Marble with interbed orientation of 0°, 30°, 60°, and 90°, respectively)

3.5. Localized deforamtion evolution characteristics

During rock deformation, the high strain concentration band evolves into the fracture surface at the final loading stage. In this section, the deformation characteristics of selected high strain band are investigated. Fig.12 plots the deformation information, including Z-displacement (Fig.12a), total displacement (Fig.12b), and principal strain (Fig.12c) against experimental time. Within the localized band, the Z displacement, total displacement and principal strain all increases with the experimental time for sample having an interbed orientation of 90° and 60°, however, they show a first increase and then a decrease trend for the 30° interbed sample. The total displacement and principal strain is relatively large for sample with interbed orientation of 30° and 60° than sample with orientation of 0° and 90°. It is the largest for the 30° interbed sample, indicating that the strain localization takes places progressively and develops fast for this sample, therefore, the capacity of resist deformation for it is the weakest. The differential deformation of the high strain concentration implies the influence of interbed structure on rock damage and the associated failure mode.

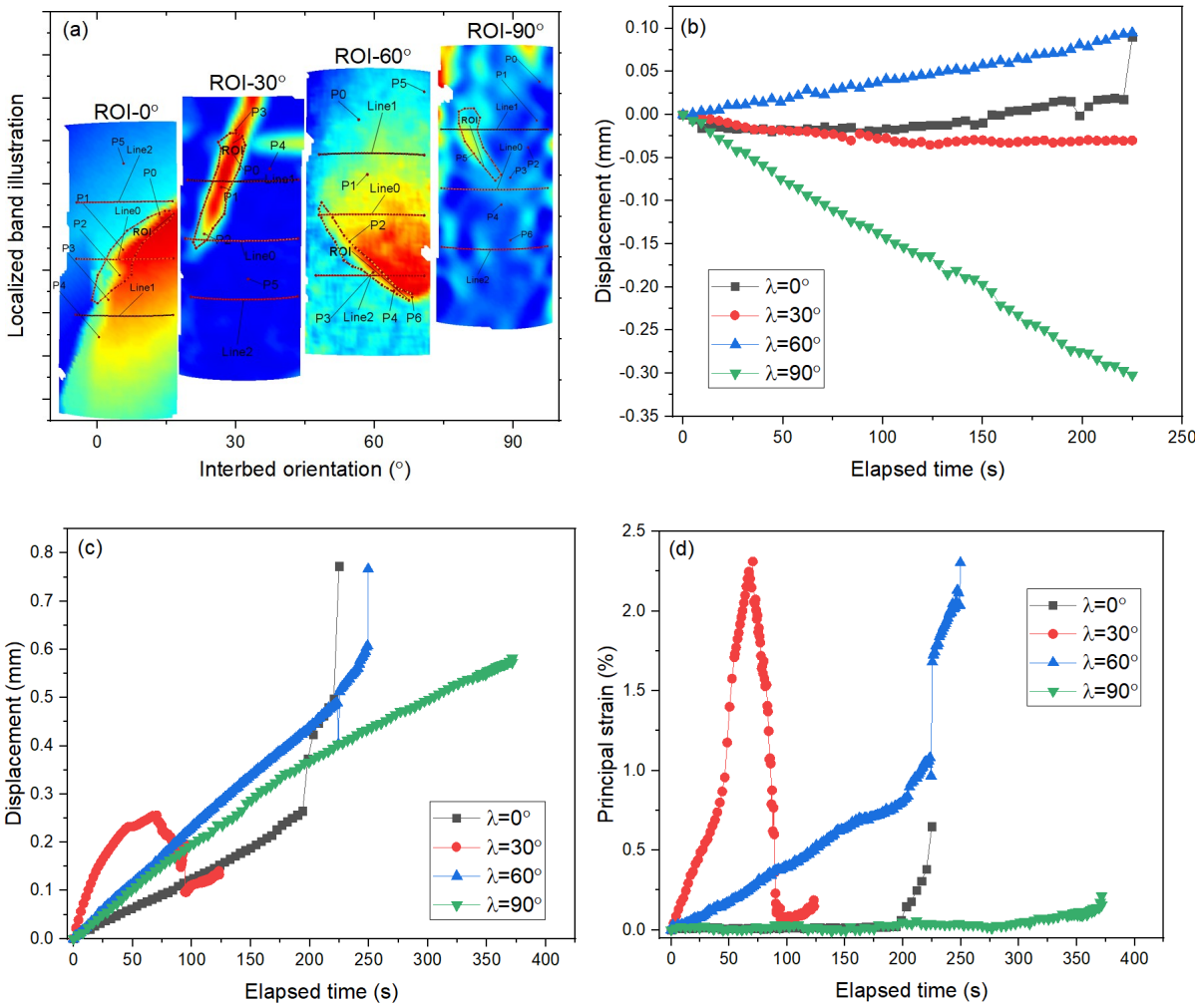

Fig.12 Depicts of the field deformation for the regions of interest (ROI) located at the strain bands. a:Selction of ROIs for the tested marble; b-d: Plots of the Z-displacement, total displacement (b), principal strain and the experimental time for the tested marble samples, respectively.

4. Discussions

The rock in nature commonly contains massive inherent discontinuities which include the layers, joints, faults, foliations and cleavages, etc. The integrity and mechanical behaviors of rock are all determined by those initial defects [1-3]. Interbed, as a typical geological discontinuity, is sound developed in many kinds of rocks, such as marble, shale, mudstone, slate, etc. Plenty of efforts have been performed to reveal the anisotropic geomechanical behaviors of interbedded rock, the previous effects are mainly focused on the anisotropy of rock deformation, strength, elastic modulus, P-wave or S-wave velocities, et al. In addition, mesoscopic physical and mechanical testings, including SEM scanning, real-time CT scanning, have also been conducted to reveal the mesoscopic anisotropic characteristics. However, the studies regarding to the whole-process deformation evolution pattern are rarely reported.

In this work, 3D DIC technique was employed to reveal the anisotropic strain evolution characteristics of interbedded marble obtained from an open pit slope. The influence of rock structure, especially the interbeds, on rock full-field displacement and strain evolution were analyzed. The influence of stiffness difference between rock matrix and interbed on strain evolution was first illustrated. The testing results highlight the influence of interbed structure on the distribution of displacement and strain and the associated failure mode. It is proved that the contact surface between the rock matrix and interbed is the weakest part of rock. The displacement or strain monitoring in the section lines, key points and the localized bands further clarify the anisotropic strain evolution impacted by the interbed structure. It should be noted that the full-field strain measurement in this work reveals the strain evolution of rock surface facing to the two high speed cameras, the volumetric strain of the r around the whole rock should be revealed in the further studies. In addition, the 3D DIC technique is based on the continuum theory, it gains an insight of the whole deformation process on rock surface, the crack initiation, propagation and coalescence behaviors should be deeply revealed by other nondestructive technologies.

5. Conclusions

In this paper, three-dimensional digital image correlation (3D DIC) method was employed to investigate the anisotropic field strain evolution of interbedded marble under uniaxial compressive loads. The full-field displacement and strain patterns in different stages of rock failure were successfully captured during the whole process. The conclusions are drawn below.

(1) The 3D DIC system realized the capture of the field strains and damage evolution for marble with different interbed orientation. The acquisition results enhance the understanding of anisotropic deformation behaviors and the progressive failure process of marble.

(2) The interbed within rock influences the displacement development and high strain concentration pattern. Different stress strain responses can be generated depending on the interbed structure. It is shown that shear sliding instability occurs for a sample with 30° interbed orientation and the strength of it is the minimum.

(3) The field displacement monitored from the section line and key points display distinct pattern and is impacted by interbed orientation. The field displacement evolution curves present different pattern and are impacted by the localized deformation.

(4) Field strain development in rock suggests that strain localization takes places progressively and develops at a low rate for the 0° and 90° interbed rock, and a high rate for the 30° and 60° interbed rock. The results show that the failure modes are respectively tension destruction for 0° interbed rock, a mixed tension-shear destruction for rock with 60° and 90° interbed orientation and pure shear destruction for rock that having 30° interbed orientation.

Acknowledgements

This study was supported by National key technologies Research & Development program (2018YFC0808402), Beijing Natural Science Foundation (8202033), the Fundamental Research Funds for the Central Universities (FRF-TP-20-004A2).

Conflict of interest: The authors declare no conflict of interest.

References

[1] Wang, Y., Feng, W. K., Wang, H. J., Li, C. H., & Hou, Z. Q. (2020). Rock bridge fracturing characteristics in granite induced by freeze-thaw and uniaxial deformation revealed by AE monitoring and post-test CT scanning. Cold Regions Science and Technology, 103115.

[2] Wang, Y., Li, C., Han, J., & Wang, H. (2020). Mechanical behaviours of granite containing two flaws under uniaxial increasing–amplitude fatigue loading conditions: An insight into fracture evolution analyses. Fatigue & Fracture of Engineering Materials & Structures, 43(9), 2055-2070.

[3] Detournay E (1986) Elastoplastic model of a deep tunnel for a rock with variable dilatancy. Rock Mech Rock Eng 19(2):99-108

[4] Yu, L., & Liu, J. (2015). Stability of interbed for salt cavern gas storage in solution mining considering cusp displacement catastrophe theory. Petroleum, 1(1), 82-90.

[5] Cała, M., Cyran, K., Kowalski, M., & Wilkosz, P. (2018). Influence of the anhydrite interbeds on a stability of the storage caverns in the Mechelinki salt deposit (Northern Poland). Archives of Mining Sciences, 63.

[6] Ozturk, H., & Altinpinar, M. (2017). The estimation of uniaxial compressive strength conversion factor of trona and interbeds from point load tests and numerical modeling. Journal of African Earth Sciences, 131, 71-79.

[7] Wang, G., Guo, K., Christianson, M., & Konietzky, H. (2011). Deformation characteristics of rock salt with mudstone interbeds surrounding gas and oil storage cavern. International Journal of Rock Mechanics and Mining Sciences, 48(6), 871-877.

[8] Tommasi, P., Verrucci, L., Campedel, P., Veronese, L., Pettinelli, E., & Ribacchi, R. (2009). Buckling of high natural slopes: The case of Lavini di Marco (Trento-Italy). Engineering Geology, 109(1-2), 93-108.

[9] Zhao, Z., Li, X., He, J., Mao, T., Zheng, B., & Li, G. (2018). A laboratory investigation of fracture propagation induced by supercritical carbon dioxide fracturing in continental shale with interbeds. Journal of Petroleum Science and Engineering, 166, 739-746.

[10] Wang, Y., Li, X., Zhang, B., & Zhao, Z. (2016). Optimization of multiple hydraulically fractured factors to maximize the stimulated reservoir volume in silty laminated shale formation, Southeastern Ordos Basin, China. Journal of Petroleum Science and Engineering, 145, 370-381.

[11] Wang, Y., Tan, W. H., Liu, D. Q., Hou, Z. Q., & Li, C. H. (2019). On anisotropic fracture evolution and energy mechanism during marble failure under uniaxial deformation. Rock Mechanics and Rock Engineering, 52(10), 3567-3583.

[12] Wang, Y., Gao, S., Liu, D., & Li, C. (2020). Anisotropic fatigue behaviour of interbeded marble subjected to uniaxial cyclic compressive loads. Fatigue & Fracture of Engineering

Materials & Structures, 43(6), 1170-1183.
[13] Wang, Y., Hu, Y. Z., & Gao, S. H. (2020). Dynamic mechanical behaviors of interbedded marble subjected to multi-level uniaxial compressive cyclic loading conditions: An insight into fracture evolution analysis. Engineering Fracture Mechanics, 107410.
[14] Fournier, B., Bérubé, M. A., & Bergeron, G. (1991). A rapid autoclave mortar bar method to determine the potential alkali-silica reactivity of St. Lawrence lowlands carbonate aggregates (Quebec, Canada). Cement, concrete and aggregates, 13(1), 58-71.
[15] Zhao, Z., Li, X., Wang, Y., Zheng, B., & Zhang, B. (2016). A laboratory study of the effects of interbeds on hydraulic fracture propagation in shale formation. Energies, 9(7), 556.
[16] Wang, Y., Meng, H., & Long, D. (2021). Experimental investigation of fatigue crack propagation in interbedded marble under multilevel cyclic uniaxial compressive loads. Fatigue & Fracture of Engineering Materials & Structures, 44(4), 933-951.
[17] Hirono, T., Takahashi, M., & Nakashima, S. (2003). In situ visualization of fluid flow image within deformed rock by X-ray CT. Engineering Geology, 70(1-2), 37-46.
[18] Wang, Y., Feng, W. K., & Li, C. H. (2020). On anisotropic fracture and energy evolution of marble subjected to triaxial fatigue cyclic-confining pressure unloading conditions. International Journal of Fatigue, 134, 105524.
[19] Poszytek, A., Mikołajewski, Z., & Dohnalik, M. (2016). X-ray micro computed tomography characterization of porosity in Rotliegend sandstones on the northern slope of the Wolsztyn Ridge, western Poland. Geological Quarterly, 60(4), 801-810.
[20] Tang, Y., Okubo, S., Xu, J., & Peng, S. (2019). Progressive failure behaviors and crack evolution of rocks under triaxial compression by 3D digital image correlation. Engineering geology, 249, 172-185.
[21] Munoz, H., & Taheri, A. (2017). Specimen aspect ratio and progressive field strain development of sandstone under uniaxial compression by three-dimensional digital image correlation. Journal of Rock Mechanics and Geotechnical Engineering, 9(4), 599-610.
[22] Sharafisafa, M., Shen, L., & Xu, Q. (2018). Characterisation of mechanical behaviour of 3D printed rock-like material with digital image correlation. International Journal of Rock Mechanics and Mining Sciences, 112, 122-138.
[23] Xing, H. Z., Zhang, Q. B., Ruan, D., Dehkhoda, S., Lu, G. X., & Zhao, J. (2018). Full-field measurement and fracture characterisations of rocks under dynamic loads using high-speed three-dimensional digital image correlation. International Journal of Impact Engineering, 113, 61-72.
[24] Munoz, H., Taheri, A., & Chanda, E. K. (2016). Pre-peak and post-peak rock strain characteristics during uniaxial compression by 3D digital image correlation. Rock Mechanics and Rock Engineering, 49(7), 2541-2554.
[25] M.A. Sutton, J.J. Orteu, H. Schreier, Image correlation for shape, motion and deformation measurements: basic concepts, theory and applications, Springer Science & Business Media, 2009.
[26] Y. Tang, S. Okubo, J. Xu, S. Peng, Progressive failure behaviors and crack evolution of rocks under triaxial compression by 3D digital image correlation, Eng. Geol. 249 (2019) 172–185.
[27] Hao, J., Qiao, L., Li, Z., & Li, Q. (2021). Study on the fracture behavior of prefabricated fissures granite based on DIC and laser scanning techniques. Fatigue & Fracture of

Engineering Materials & Structures.
[28] Song, H., Zhang, H., Fu, D., Kang, Y., Huang, G., Qu, C., & Cai, Z. (2013). Experimental study on damage evolution of rock under uniform and concentrated loading conditions using digital image correlation. Fatigue & Fracture of Engineering Materials & Structures, 36(8), 760-768.